RSC Advances

ROYAL SOCIETY OF CHEMISTRY

www.rsc.org/advances

Evaluation of Ba-deficient $PrBa_{1-x}Fe_2O_{5+\delta}$ oxides as cathode materials for intermediate-temperature solid oxide fuel cells

Tao Chen[a,b], Shengli Pang[a*], Xiangqian Shen[a,b], Xuening Jiang[c], Wenzhi Wang[a,b]

[a] *Institute for Advanced Materials, Jiangsu University, Zhenjiang 212013, R. P. China*

[b] *School of Material Science & Engineering, Jiangsu University, Zhenjiang 212013, R. P. China*

[c] *Key Laboratory of Materials Modification by Laser, Ion and Electron Beams, Ministry of Education, Dalian University of Technology, Dalian 116024, R. P. China*

Abstract

Cobalt-free double perovskite oxides are promising cathode materials in intermediate-temperature solid oxide fuel cells, and often suffer from a low activity in oxygen reduction reactions. Here, we report on Ba deficiency as an effective strategy to enhance the electrochemical performance of cobalt-free double perovskite $PrBaFe_2O_{5+\delta}$, which is properly related to the formation and redistribution of oxygen vacancies in double perovskite. The effect of Ba deficiency on crystal structure, surface properties, oxygen content, electrical conductivity, thermal expansion, chemical compatibility with gadolinium-doped ceria ($Gd_{0.1}Ce_{0.9}O_{1.95}$) electrolyte, microstructure, and electrochemical performance of $PrBa_{1-x}Fe_2O_{5+\delta}$ (x = 0.00–0.03) was evaluated systematically. Our preliminary results suggest that Ba deficiency is a feasible means to tailor the physico- and electrochemical properties of cobalt-free double perovskite, and that $PrBa_{0.97}Fe_2O_{5+\delta}$ is a potential cathode material for intermediate-temperature solid oxide fuel cells.

* Corresponding author. Tel./Fax: 86-0511-88791964; E-mail: slpang@ujs.edu.cn (S. Pang).

1. Introduction

The energy crisis and environmental problems caused primarily by the current widespread and inefficient use of fossil fuels has intensified the need for new energy conversion devices. Among available technologies capable of converting stored chemical energy to usable electrical energy, solid oxide fuel cells (SOFCs) offer an unmatched working efficiency, low gaseous pollutant emissions, and excellent fuel flexibility, and are considered to represent a key component of future energy solutions.[1,2] One strategy that has been proposed for the commercialization of SOFCs, while achieving enhanced durability and cost reduction, is to lower the working temperature to an intermediate temperature (IT) range of 600–800 °C. At these lower temperatures, however, increased polarization resistance at the cathode that results from a high oxygen reduction reaction (ORR) activation energy, becomes the primary factor that determines the overall cell performance. Thus, the exploration of novel cathode materials with high catalytic activity for ORR is of significant importance in IT-SOFC development.

In recent years, double perovskites with general formula $LnBaCo_2O_{5+\delta}$ (Ln = lanthanide) have been proposed as potential cathode materials for IT-SOFCs owing to their rapid oxygen surface exchange, bulk diffusion kinetics, and high electrical conductivities. These oxides possess 112-type perovskite structures with alternating stacking layers of $[CoO_2]$-$[LnO_\delta]$-$[CoO_2]$-[BaO] along the c-axis. This periodic structure is expected to reduce the oxygen ion transport activation energy along the ab plane significantly and has been reported to enhance the oxygen transport rate effectively compared with transport rates exhibited by disordered counterparts of these materials.[3,4] The structural, thermal, electrical,

and electrochemical properties of double perovskites have thus been studied extensively.[5-10] Unfortunately, as for other cobalt-based perovskites, the thermal expansion coefficient (TEC) of $LnBaCo_2O_{5+\delta}$ from 30–900 °C (such as 23.4×10^{-6} $^oC^{-1}$ for $PrBaCo_2O_{5+\delta}$)[8] is much larger than that of commonly used electrolytes ($10–13\times10^{-6}$ $^oC^{-1}$)[11] and sealing materials ($11–14\times10^{-6}$ $^oC^{-1}$)[12]. This leads to a significant thermal mismatch that can produce interfacial stresses between the cathode and other components, and lead to cell cracking and degradation. The volatility of these compounds at elevated temperatures and the relatively high price of cobalt also limit the practical application of $LnBaCo_2O_{5+\delta}$ as cathode material for IT-SOFCs. Substituting other, more readily available transition metals such as iron and nickel for cobalt may provide a solution to these challenges.[13-19] As an example, monotonic decreases in TEC of $LnBaCo_{2-x}Fe_xO_{5+\delta}$ (Ln = Nd or Gd) with increasing Fe content were observed by Kim et al.[13] and are attributed to the increased strength of the Fe-O bond compared with the Co-O bond and the reduced contribution of the low- to high-spin transition of Co^{3+} to TEC. The thermal and chemical compatibilities between $PrBaCo_{2-x}Fe_xO_{5+\delta}$ and $Sm_{0.2}Ce_{0.8}O_{1.90}$ electrolyte were reported to be improved by Fe substitution for Co.[13,14] For this reason, various series of cobalt-free double perovskites have been proposed, such as $PrBaFe_2O_{5+\delta}$,[13-16] $NdBaFe_2O_{5+\delta}$,[15,17] and $GdBaFe_2O_{5+\delta}$,[15,18,19] as potential cathode materials for IT-SOFCs. However, since Fe ions are less conductive and more stable than Co ions, cobalt-free double perovskites often experience significant decreases in electrical conductivity and electrochemical catalytic activity in the ORR compared with cobalt-based double perovskites such as $LnBaCo_2O_{5+\delta}$. Therefore, it is important to establish feasible strategies to enhance the electrochemical performance of cobalt-free double perovskites.

The introduction of A-site cationic deficiencies is a useful means of modifying the physical and chemical properties of perovskite oxides.[8,20-26] For example, Liu et al.[20] and Yang et al.[21] observed gradual increases in electrical conductivity and catalytic activity for ORR as the extent of Ba deficiency in $Ba_{1-x}Co_{0.7}Fe_{0.2}Ni_{0.1}O_{3-\delta}$ was increased from x = 0.00 to 0.15. In addition, maximum power density values of 1062 mW cm^{-2} (600 °C) and 1139 mW cm^{-2} (650 °C) were obtained for $Ba_{1-x}Co_{0.7}Fe_{0.2}Ni_{0.1}O_{3-\delta}$ (x = 0.10) oxide. Our group has found that A-site Ba-deficient cobalt-based double perovskites $LnBaCo_2O_{5+\delta}$ (Ln = La or Pr) show a significantly enhanced electrochemical performance.[8,22,23] For example, Ba-deficient $PrBa_{1-x}Co_2O_{5+\delta}$ (x = 0.08) oxide exhibits a polarization resistance from 600–700 °C that is approximately half that of the stoichiometric oxide $PrBaCo_2O_{5+\delta}$. This effect likely originates from the generation of additional oxygen vacancies in Ba-deficient oxides that facilitate two-dimensional layer diffusion of oxygen along the ab plane and interlayer diffusion along the c-axis.[8,22,24,25] A-site cation deficiency is expected to be an effective means to improve the electrochemical performance of cobalt-based double perovskites. However, since the physical and chemical properties of oxides are determined by their compositions at the A and B sites, no reports exist to data on the effects of A-site deficiencies on the properties of cobalt-free double perovskite $LnBaFe_2O_{5+\delta}$ with regard its application as cathode material for IT-SOFCs.

We studied the effects of Ba deficiency on crystal structure, oxygen non-stoichiometry, electrical conductivity, thermal expansion, and electrochemical performance of $PrBa_{1-x}Fe_2O_{5+\delta}$. Preliminary results suggest that cobalt-free double perovskite $PrBa_{1-x}Fe_2O_{5+\delta}$, in which the Ba deficiency is x = 0.03, is a promising cathode material for IT-SOFCs.

2. Experimental

Cobalt-free double perovskites $PrBa_{1-x}Fe_2O_{5+\delta}$ (x = 0.00–0.10) were synthesized via a combined ethylene diamine tetraacetic acid (EDTA)/citric acid sol–gel method that has been described in detail in our previous publications.[8,22] Briefly, the desired amount of metal nitrites ($Pr(NO_3)_3 \cdot 6H_2O$, $Ba(NO_3)_2$, and $Fe(NO_3)_2 \cdot 6H_2O$, all analytical grade) was dissolved in an EDTA/$NH_3 \cdot H_2O$ solution (~pH 6) with heating and stirring, after which a citric acid/$NH_3 \cdot H_2O$ solution (~pH 6) was added at a total metal ion:EDTA:citric acid molar ratio of 1:1:2. The resulting solution was evaporated at 80 °C over several hours to obtain a viscous gel. The obtained gels were pre-calcined at 250 °C and then calcined in air at 1200 °C for 7 h to generate a double perovskite structure.

The phase structures of the as-synthesized $PrBa_{1-x}Fe_2O_{5+\delta}$ (x = 0.00–0.10) powders and calcined $PrBa_{1-x}Fe_2O_{5+\delta}$-gadolinium-doped ceria ($Gd_{0.1}Ce_{0.9}O_{1.95}$, GDC) mixtures were characterized by X-ray diffraction (XRD; Rigaku D/Max 2400) from a 2θ of 20–80°. Oxygen contents of the $PrBa_{1-x}Fe_2O_{5+\delta}$ (x=0.00-0.03) oxides at various temperature were characterized by iodometric titration method[27,28] and thermo-gravimetric analysis (TGA; Netzsch STA449C). Before the iodometric titration and TGA measurements, the $PrBa_{1-x}Fe_2O_{5+\delta}$ (x=0.00-0.03) powders were vacuum dried at 100 ^oC for 4 h to remove the surface absorbed gases (i.e. H_2O, CO_2 et al.). The TGA was conducted in air, fabricated by mixing high purity N_2 and O_2 in the volume ratio of 79:21, from room temperature to 900 ^oC at a heating rate of 2 $^oC\ min^{-1}$. Conductivity data were acquired in air from 300–800 °C using a direct current (DC) four-electrode method. The chemical state of the transition metal ions was characterized by a multifunctional imaging electron spectrometer (Thermo ESCALAB 250XI) with a monochromatized microfocused Al

Kα (1486.6 eV) radiation source. Thermal expansion data were obtained in air using a dilatometer (Netzsch DIL 402PC) with a heating rate of 2 °C min^{-1} from 30–900 °C. The electrochemical performance of the $PrBa_{1-x}Fe_2O_{5+\delta}$ (x = 0.00-0.03) oxides were characterized by electrochemical impedance spectra, using GDC as the electrolyte in a $PrBa_{1-x}Fe_2O_{5+\delta}$/GDC/$PrBa_{1-x}Fe_2O_{5+\delta}$ symmetrical cell configuration. Dense GDC disks (diameter: ~10 mm, thickness: ~1 mm) were prepared by pressing GDC powder uniaxially at 200 MPa followed by sintering at 1280 °C for 4 h. Slurries that were prepared by mixing the cathode powders with α-terpineol and ethyl cellulose were screen-printed onto both sides of the GDC disks and the disks were then calcined at 1000 °C for 2 h to obtain porous cathode layers. Electrochemical impedance spectra data for these symmetrical cells were collected using a multi-channel potentiostat/galvanostat (VMP2) with integrated frequency response analyzer (Biologic) by applying an open circuit voltage from 0.1 Hz to 0.1 MHz. Morphologies of the post-test cells were analyzed by field emission scanning electron microscopy (FESEM, JSM-7001F). The specific surface area and pore size distribution of the cathode layers were measured by Brunauer-Emmett-Teller (BET) adsorption-desorption isotherms of N_2 technology with an automatic analyzer (Nova 3000e, Quantachrome). Single cells with the configuration of Ni-YSZ/YSZ/GDC/$PrBa_{1-x}Fe_2O_{5+\delta}$ were fabricated by screen printed cathode slurry onto the commercial Ni-YSZ/YSZ/GDC half cells (NingBo SOFCMAN Energy Technology Co., Ltd) and calcined at 1100 ^oC for 2 h. The as-obtained single cells were sealed on one side of alumina tube with the help of silver paste (DAD-87, Shanghai Institute of Synthesized Risen) and then assembled to the home-made cell test system. The current-voltage (I-V) and current-power (I-P) curves were collected by a

Solartron 1287 potentiostat with humidified H_2 (~100 ml min^{-1}) as fuel and flowing air as oxide.

3. Results and discussion

3.1. Phase structure

XRD patterns of the $PrBa_{1-x}Fe_2O_{5+\delta}$ (x = 0.00–0.10) powders after calcined at 1200 °C for 7 h in air are shown in Figure 1. As can be seen from Figure 1a and from the data in Table 1, highly crystalline, layered perovskite phases with an orthorhombic lattice geometry and Pmmm space group were obtained for each $PrBa_{1-x}Fe_2O_{5+\delta}$ oxide. The structural parameters of the cation stoichiometric $PrBaFe_2O_{5+\delta}$ are comparable with previously reported results.[13,16] The diffraction peaks were observed to shift to higher angles (Figure 1b) with increase in Ba deficiency (x), which suggests lattice shrinkage (Table 1). A Pr_6O_{11} impurity phase (JCPDS# 42-1121) can be identified based on minor diffraction peaks that appear at approximately 28° in samples for which x = 0.05–0.10, which indicates that the value of the A-site Ba deficiency fraction (x) was limited to approximately 0.03 in the $PrBa_{1-x}Fe_2O_{5+\delta}$ oxides. Therefore, evaluation hereafter in this paper focuses on samples with x = 0.00 and 0.03.

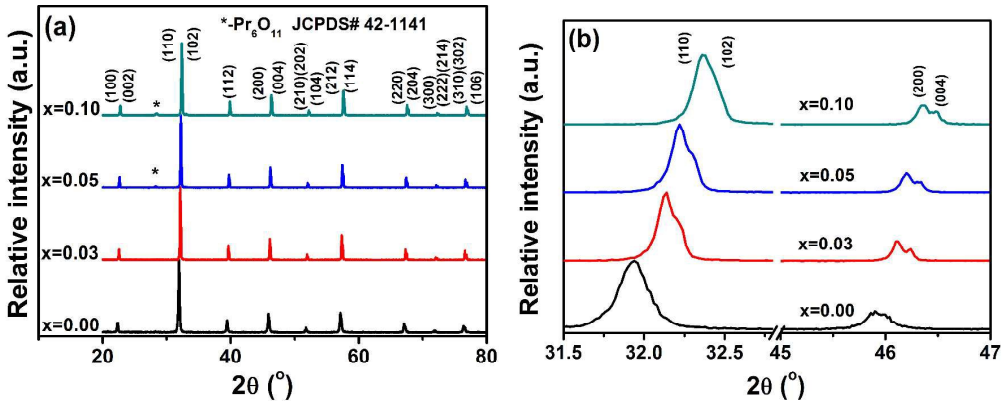

Figure 1 Whole (a) and magnified (b) XRD patterns of $PrBa_{1-x}Fe_2O_{5+\delta}$ (x = 0.00–0.10)

powders calcined at 1200 °C for 7 h in air.

Table 1 Lattice parameters of $PrBa_{1-x}Fe_2O_{5+\delta}$ (x = 0.00–0.10) oxides.

Samples	Space group	a (Å)	b(Å)	c (Å)	V ($Å^3$)
x = 0.00	Pmmm	3.952	3.979	7.869	123.740
x = 0.03	Pmmm	3.932	3.943	7.839	121.535
x = 0.05	Pmmm	3.927	3.929	7.850	121.119
x = 0.10	Pmmm	3.900	3.921	7.829	119.720

3.2 X-ray photoelectron spectroscopy analysis

To identify the surface properties of $PrBaFe_2O_{5+\delta}$ and $PrBa_{0.97}Fe_2O_{5+\delta}$, the chemical state of elemental O, Pr, and Fe was measured by X-ray photoelectron spectroscopy (XPS) and normalized with a C1s peak to 284.6 eV. Figure 2 shows the O1s XPS spectra and fitting curves of $PrBaFe_2O_{5+\delta}$ and $PrBa_{0.97}Fe_2O_{5+\delta}$. Three distinguishable peaks with binding energies from 528.5–533.0 eV are visible. The peak at 528.5 eV is characterized by lattice O^{2-} ions (O_L) of the perovskite structure, whereas the other two peaks with binding energy of 530.9 and 533.0 eV probably originate from carbonate structures (O_C) and hydroxyl groups (O_H).[29-32] The appearance of peaks at 530.9 and 533.0 eV indicates the reactivity of $PrBaFe_2O_{5+\delta}$ and $PrBa_{0.97}Fe_2O_{5+\delta}$ with CO_2 and H_2O when exposed to ambient atmosphere, respectively. A similar phenomenon was observed in other perovskite-based materials and is reported to be closely related to the existence of alkaline-earth elements in the materials.[29,31,32]

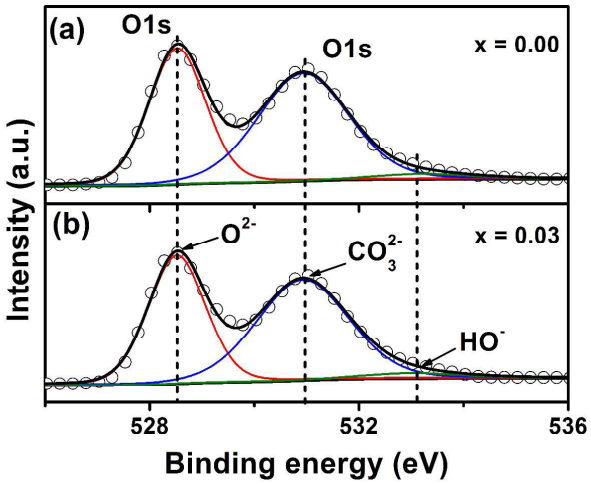

Figure 2 O 1s core-level spectra and fitted lines of $PrBa_{1-x}Fe_2O_{5+\delta}$ at room temperature: (a) x = 0.00 and (b) x = 0.03.

Figure 3 shows Pr 3d core-level spectra and corresponding fitting curves of $PrBaFe_2O_{5+\delta}$ and $PrBa_{0.97}Fe_2O_{5+\delta}$ samples at room temperature. The main peaks with binding energy of 932.2–932.5 eV and 952.9–953.1 eV can be assigned to Pr^{4+} $3d_{5/2}$ and $3d_{3/2}$, whereas the peak pairs located at ~928.0/933.6 eV and 949.0/956.4 eV originate from Pr^{3+} $3d_{5/2}$ and $3d_{3/2}$.[29,33] A similar result was also observed by Jin et al. in double perovskite $PrBaCo_{2/3}Fe_{2/3}Cu_{2/3}O_{5+\delta}$[30] and indicated the coexistence of mixed valences of Pr^{4+} and Pr^{3+} in $PrBaFe_2O_{5+\delta}$ and $PrBa_{0.97}Fe_2O_{5+\delta}$ samples. Pr^{4+} is the dominant chemical state of Pr in both samples as is characterized by the main spectrum at 932.2–932.5 eV and 952.9–953.1 eV.

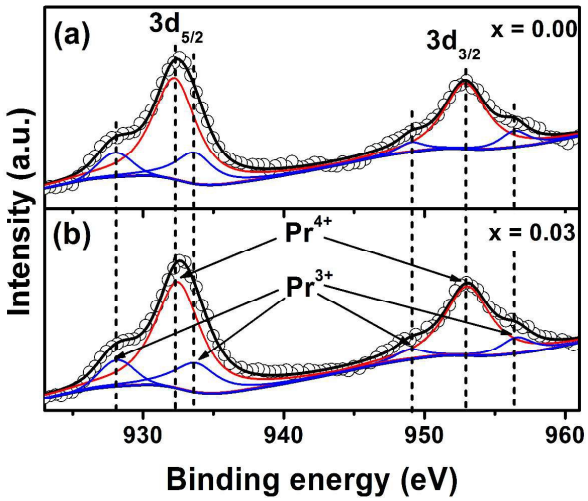

Figure 3 Pr 3d core-level spectra and fitted lines of $PrBa_{1-x}Fe_2O_{5+\delta}$ at room temperature: (a) x = 0.00 and (b) x = 0.03.

Figure 4 shows the Fe 2d core-level spectra and corresponding fitting curves of samples of $PrBaFe_2O_{5+\delta}$ and $PrBa_{0.97}Fe_2O_{5+\delta}$ at room temperature. Double peaks at 711.2 and 724.2 eV represent Fe^{4+} $2d_{3/2}$ and $2d_{1/2}$, whereas the other set of peaks with binding energies of 709.6 and 722.9 eV represent Fe^{3+} $2d_{3/2}$ and $2d_{1/2}$, respectively.[33] The satellite peak with binding energy of 717.5 eV can be ascribed to the Fe^{3+} species.[30,33] No peak related to the Fe^{2+} species was observed in the XPS spectra, which indicates that the valences of Fe in both samples are 3+ and 4+.

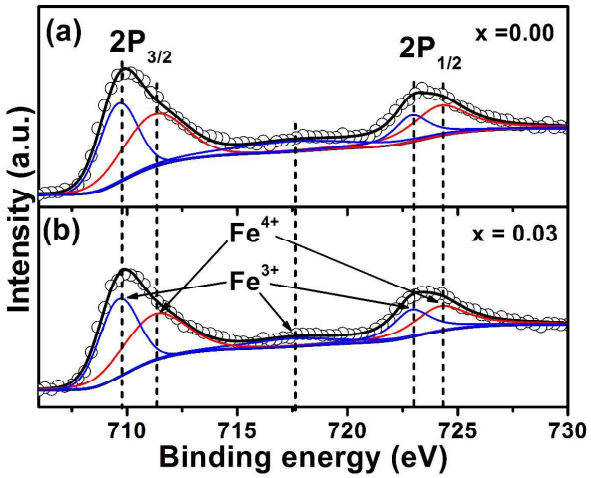

Figure 4 Fe 2p core-level spectra and fitted lines of $PrBa_{1-x}Fe_2O_{5+\delta}$ at room temperature: (a) x = 0.00 and (b) x = 0.03.

Based on the fitting results of the XPS spectra for O 1s, Pr 3d, and Fe 2p, the integrated intensity ratios of $O_L/(O_C+O_H)$, Pr^{4+}/Pr^{3+}, and Fe^{4+}/Fe^{3+} were calculated and are given in Table 2. Within the experimental error, no detectable changes are observed for $O_L/(O_C+O_H)$ and Pr^{4+}/Pr^{3+}. Compared with the parent perovskite ($PrBaFe_2O_{5+\delta}$), a slight decrease in Fe^{4+} ratio was observed for the $PrBa_{0.97}Fe_2O_{5+\delta}$ sample, which suggests that the introduction of Ba deficiency to the cobalt-free double perovskite results in a reduction rather than an oxidation of transition metal (Fe). To maintain the electrical neutrality of the oxide, a reduction in positive charge can be balanced by the formation of additional oxygen vacancies at the $PrBa_{0.97}Fe_2O_{5+\delta}$ surface.

Table 2

Percentage contribution from core electrons for O, Pr, and Fe.

Samples	O_L	O_c+O_H	Pr^{4+}	Pr^{3+}	Fe^{4+}	Fe^{3+}
x = 0.00	43.0%	57.0%	74.9%	25.1%	48.3%	51.7%
x = 0.03	43.0%	57.0%	74.8%	25.2%	47.7%	52.3%

3.3 Oxygen content

Oxygen contents of the $PrBa_{1-x}Fe_2O_{5+\delta}$ (x=0.00-0.03) oxides at various temperature in air were characterized by iodometric titration method and thermo-gravimetric analysis technique,[6,28] and presented in figure 5. As depicted in this figure, three distinguishable stages, the oxygen content kept constant with higher temperature (25-230 ^oC), absorption of oxygen in the surrounding atmosphere with higher temperature (230-340 ^oC), and release of lattice oxygen with higher temperature (340-900 ^oC), were observed for both samples in the measured temperature range. For the fist stage, no detectable changes in oxygen contents were observed for both samples. Similar phenomenon were observed in other perovskite oxides,[6,28] and can be attributed to the relatively low temperatures for which the oxygen ions are expect to "frozen" in the lattice of the $PrBa_{1-x}Fe_2O_{5+\delta}$ (x=0.00-0.03) oxides. For the second stage, slightly increases in oxygen contents were observed for both samples with higher temperature which properly comes from the difference in the gases oxygen content of the surrounding atmosphere between the muffler furnace (where the samples were synthesized) and the TGA furnace (where the samples were tested). Gradually decreases in oxygen content with higher temperature were obtained in the third stage which properly related to the thermal induced release of lattice oxygen.[6,28] Furthermore, at a given temperature, $PrBa_{1-x}Fe_2O_{5+\delta}$ (x=0.03) exhibits much lower oxygen contents than that of the parent oxide ($PrBaFe_2O_{5+\delta}$) in the measured temperature range indicating the formation of oxygen vacancies as the charge compensation for the Ba-deficiency in the cobalt-free double perovskites. It is worth noting that the formation of additional oxygen vacancies is expected to be beneficial in promoting the catalytic activity for ORR.[34]

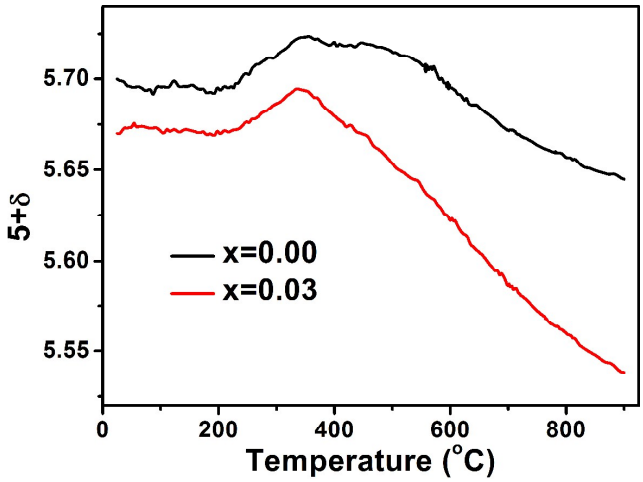

Figure 5 Oxygen content (5+δ) of $PrBa_{1-x}Fe_2O_{5+\delta}$ (x=0.00-0.03) oxides measured in air.

3.4 Electrical conductivity

Figure 6 summarizes the electrical conductivities of samples in air at various temperatures. The oxygen ion conductivity of this kind of perovskite oxide has been reported to be much lower than the electron conductivity,[10] such that the electrical conductivity described herein can be assumed to represent primarily electronic conductivity. As shown in Figure 6, all samples exhibit an initial increase in electrical conductivity from 300 to 425–450 °C, followed by a downward trend in higher temperatures. This results from thermally-induced lattice oxygen release and the formation of oxygen vacancies that hinders the mobility of electronic conduction carriers. Maximum electrical conductivities of 36 and 32 S cm^{-1} were obtained for $PrBaFe_2O_{5+\delta}$ and $PrBa_{0.97}Fe_2O_{5+\delta}$, respectively. These values are expected to be acceptable for SOFC applications since they are similar to those of previously reported cathode materials such as $Ba_{0.5}Sr_{0.5}Co_{0.8}Fe_{0.2}O_{3-\delta}$,[35,36] $Ba_{0.5}Sr_{0.5}Fe_{0.8}Cu_{0.2}O_{3-\delta}$,[37] and $Sm_{0.5}Sr_{0.5}Fe_{0.8}Cu_{0.2}O_{3-\delta}$,[38] which have comparable electrical conductivities and exhibited good

electrochemical performance. As depicted in Figure 6, $PrBa_{0.97}Fe_2O_{5+\delta}$ exhibiter a lower conductivity than the parent material within the measured temperature range, which suggests that the introduction of a Ba deficiency results in a decrease in electron conductivity in the cobalt-free double perovskite. A similar trend was observed for the cobalt-based double perovskites $LaBa_{1-x}Co_2O_{5+\delta}$[22] and cubic perovskites $La_{0.6}Sr_{0.4-x}Co_{0.2}Fe_{0.8}O_{3-\delta}$ (x = 0.0–0.2),[10] which is ascribed to the formation of additional oxygen vacancies, allows them to act as an electron-capture defect, and affects electron conductivity negatively, with higher Ba/Sr deficiency. Generally, both additional holes and oxygen vacancies will form simultaneously in the mixed ion-electron conducting perovskites at higher A-site cationic deficiencies as charge compensation mechanisms, both of which oppositely affect the electrical conductivity. As indicated by the previously studied oxygen content results, introduction of Ba deficiency will result in an obvious increase in oxygen vacancy concentration for $PrBa_{1-x}Fe_2O_{5+\delta}$ (x=0.00-0.03) oxides. Therefore, the presently observed decrease in electrical conductivity with higher x from 0.00 to 0.03 properly related to the formation of oxygen vacancies which is the main charge compensation mechanism for the Ba deficiency.

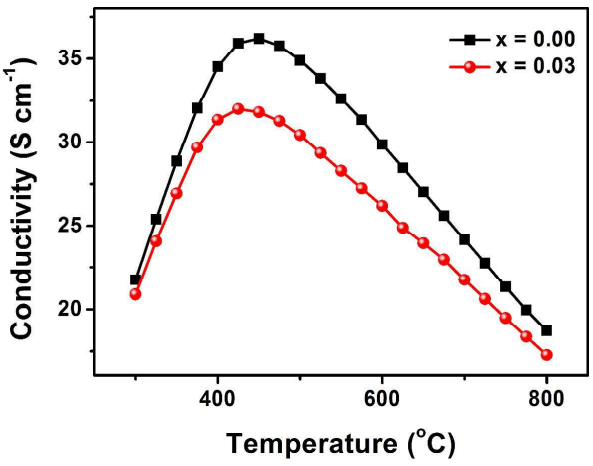

Figure 6 Electrical conductivity of $PrBa_{1-x}Fe_2O_{5+\delta}$ (x = 0.00–0.03) oxides measured in air.

3.5 Thermal expansion behavior

The thermal compatibility between cathode material and other components is another important factor that relates to the working stability of SOFCs, since a large difference in TEC between these components will introduce interfacial stress during thermal cycling and result in cracks and cell degradation. Therefore, the thermal expansion behavior of $PrBaFe_2O_{5+\delta}$ and $PrBa_{0.97}Fe_2O_{5+\delta}$ was characterized by dilatometry measurements over 30–900 °C. The obtained thermal expansion curves and calculated TEC values are presented in Figure 7. Both samples exhibit a gradual expansion with higher temperature that can be ascribed to nonharmonic atomic vibrations, dependent on electrostatic attraction forces within the lattice, and chemical expansion induced by the thermal reduction of iron ions to the lower valence state.[21,26] An average TEC value as low as 16.1×10^{-6} °C^{-1} was obtained for the $PrBaFe_2O_{5+\delta}$ oxide from 30–900 °C, which is comparable to that reported by Zhao et al.[13] and is much lower than that of the corresponding cobalt-based double perovskite $PrBaCo_2O_{5+\delta}$ (23.4×10^{-6} °C^{-1}).[8] This suggests that complete substitution of cobalt by iron can decrease the thermal mismatch between the double perovskite and GDC electrolyte significantly. A Ba deficiency results in a smaller TEC (15.2×10^{-6} °C^{-1}) compared with the parent sample. Similar trends have been reported by Zhou et al.[26] for $(Ba_{0.5}Sr_{0.5})_{1-x}Co_{0.8}Fe_{0.2}O_{3-\delta}$ and by Hansen et al.[39] for $(La_{0.6}Sr_{0.4})_{1-x}Fe_{0.8}Co_{0.2}O_{3-\delta}$ perovskites, and may be ascribed to the increased electrostatic attractions from lattice shrinkage that accompanies higher levels of Ba deficiency (Figure 1).

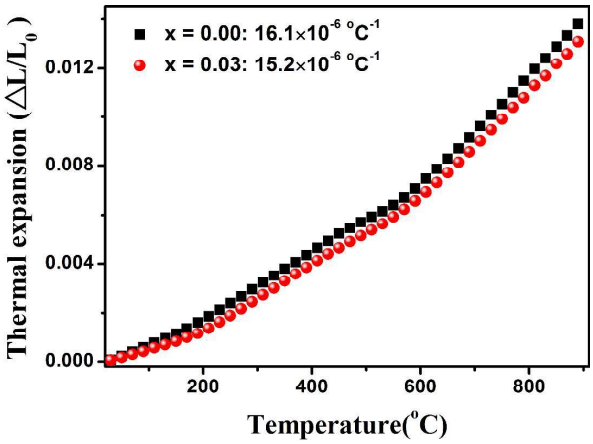

Figure 7 Thermal expansion curves of $PrBa_{1-x}Fe_2O_{5+\delta}$ (x = 0.00–0.03) oxides measured in air.

3.6 Chemical compatibility with GDC electrolyte

The chemical compatibility between cathode and various electrolytes is key with regards the long-term working stability of SOFCs, since these two components may react to form insulating phases at elevated temperatures.[13] Therefore, chemical compatibilities between double perovskites and the GDC electrolyte were characterized by mixing materials at a 1:1 mass ratio followed by calcined at 1000 °C for 2 h. The resulting mixtures were characterized by XRD to assess any reactivity. As an example of a typical result, the XRD pattern of a calcined $PrBa_{0.97}Fe_2O_{5+\delta}$-GDC powder is presented in Figure 8 with those of pure $PrBa_{0.97}Fe_2O_{5+\delta}$ and GDC powders provided for comparison. The diffraction peaks that result from the $PrBa_{0.97}Fe_2O_{5+\delta}$-GDC mixture can be indexed to a simple combination of $PrBa_{0.97}Fe_2O_{5+\delta}$ and GDC without any evidence of impurities and with no noticeable peak shifts, which suggests that the $PrBa_{1-x}Fe_2O_{5+\delta}$ oxides are chemically compatible with the GDC electrolyte at 1000 °C.

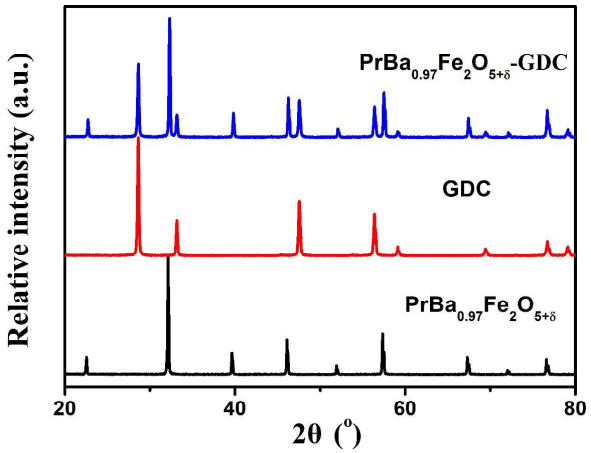

Figure 8 XRD patterns of as-synthesized $PrBa_{0.97}Fe_2O_{5+\delta}$, commercial GDC, and $PrBa_{0.97}Fe_2O_{5+\delta}$-GDC mixtures after being heat-treated at 1000 °C for 2 h.

3.7 Polarization resistance

The electrochemical activity of the $PrBa_{1-x}Fe_2O_{5+\delta}$ (x=0.00-0.03) oxides were characterized via EIS measurements with the symmetrical cell configuration $PrBa_{1-x}Fe_2O_{5+\delta}$/GDC/$PrBa_{1-x}Fe_2O_{5+\delta}$. Because the measured area specific resistances (ASRs) are microstructure-sensitive, the structural properties of the cells after EIS testing were characterized by SEM and BET adsorption-desorption isotherms of N_2 technology. Similar microstructures were observed for all the samples and a typical $PrBa_{0.97}Fe_2O_{5+\delta}$/GDC interface is presented in Figure 9a. The cathode layer, with an average thickness of approximately 16 μm, possesses a porous microstructure with uniformly distributed micro-to-nanometer sized pores that favor gas diffusion through the cathode. Good binding between the $PrBa_{0.97}Fe_2O_{5+\delta}$ cathode and the GDC electrolyte is also observed in this image, which is an important factor with regard to avoiding interfacial polarization resulting from poor interface contact. Similar specific surface area and pore size distribution were observed

for both cathode layers (Fig.9b). These features suggest the reliability for directly comparison of electrochemical activity of both samples through the presently obtained ASR values.

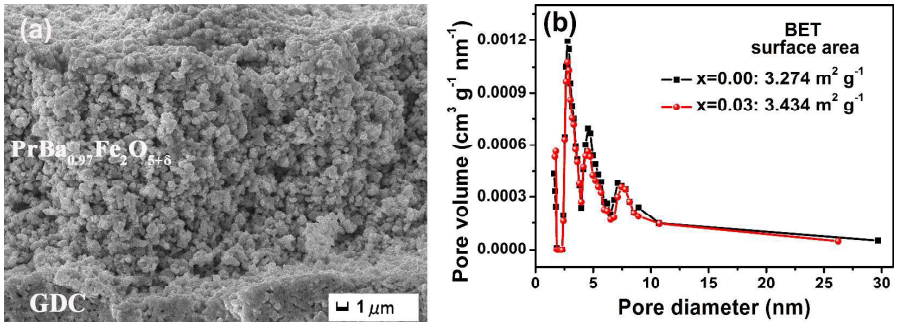

Figure 9 (a) Typical cross-sectional SEM image of the $PrBa_{0.97}Fe_2O_{5+\delta}$/GDC interface calcined at 1000 ^{o}C for 2 h in air. (b) Pore size distribution curves for both samples.

To assess the effect of Ba deficiency on the electrochemical performance of cobalt-free double perovskites, impedance spectra of the $PrBa_{1-x}Fe_2O_{5+\delta}$ (x = 0.00–0.03) oxides were acquired at 650 and 700 °C, as shown in Figure 10. In these spectra, the ohmic resistances arising from the GDC electrolyte and lead wires have been normalized to zero for clarity. The introduction of Ba deficiency results in an obvious decrease in area specific resistance (ASR) for the layered oxides. For example, an ASR value as low as 0.119 Ω cm^2 was obtained at 700 °C for $PrBa_{0.97}Fe_2O_{5+\delta}$, which is approximately 12% lower than that of the parent $PrBaFe_2O_{5+\delta}$ (0.136 Ω cm^2 at 700 °C), and indicates that the A-site Ba deficiency is an effective strategy to enhance the electrochemical performance of the cobalt-free double perovskites $PrBa_{1-x}Fe_2O_{5+\delta}$. These values are lower than those reported previously for cobalt-free cathode materials, including $SmBaFe_2O_{5+\delta}$ (0.196 Ω cm^2 at 700 °C),[15] $La_{0.6}Sr_{0.4}Ni_{0.2}Fe_{0.8}O_{3-\delta}$ (0.5 Ω cm^2 at 700 °C),[40] and $Ba_{0.5}Sr_{0.5}Zn_{0.2}Fe_{0.8}O_{3-\delta}$ (0.23 Ω cm^2 at

700 °C),[41] and are comparable or higher than those of cobalt-based perovskite cathodes such as $PrBaCo_{2/3}Fe_{2/3}Cu_{2/3}O_{5+\delta}$ (0.144 Ω cm^2 at 700 °C),[42] $PrBaCo_{1.6}Fe_{0.4}O_{5+\delta}$ (0.13 Ω cm^2 at 700 °C),[16] and $GdBaCo_{2/3}Fe_{2/3}Cu_{2/3}O_{5+\delta}$ (0.165 Ω cm^2 at 700 °C).[43] The formation and redistribution of oxygen vacancies are two possible reasons for the reduction in ASR. In terms of oxygen vacancy formation, both the oxygen content (Figure 5) and electrical results (Figure 6) obtained for the $PrBa_{1-x}Fe_2O_{5+\delta}$ oxides indicate that the formation of oxygen vacancies is the main charge compensation mechanism associated with A-site Ba deficiency with x values from 0.00 to 0.03. The presence of additional oxygen vacancies has been reported to be favorable for the ORR at the surface of the mixed ion-electronic conducting $PrBa_{1-x}Fe_2O_{5+\delta}$ and at the $PrBa_{1-x}Fe_2O_{5+\delta}$/GDC interfaces, and also promotes oxygen ion diffusion through the cathode.[34] The decrease in ASR values with A-site cation deficiency is therefore understandable. In terms of oxygen vacancy redistribution, the XRD patterns in Figure 1 show that $PrBaFe_2O_{5+\delta}$ has a similar layered structure to that of the cobalt-based double perovskites $LnBaCo_2O_{5+\delta}$ (Ln = lanthanide), in which the A-site cations Ln^{n+}/Ba^{2+} are ordered along the c axis and oxygen vacancies are restricted to the LnO and CoO layers. This structure will exhibit fast oxygen ion diffusion along the ab plane, whereas diffusion along the c axis will be forbidden.[44,45] Ba deficiencies in the cobalt-free double perovskites $PrBa_{1-x}Fe_2O_{5+\delta}$ are expected to function in a manner similar to that proposed in our previous work on cobalt-based double perovskites $LnBa_{1-x}Co_2O_{5+\delta}$ (Ln = Pr and La).[8,22] The deficiency breaks the Ba-O bonds, creates helpful additional oxygen vacancies as charge carriers for oxygen ions in the Ba-O layers, increases the possibility of oxygen ion diffusion along the c axis, shortens the oxygen diffusion length through the cathode, and results in a decrease in

ASR. This hypothesis requires further confirmation by theoretical simulation and experimental measurements.

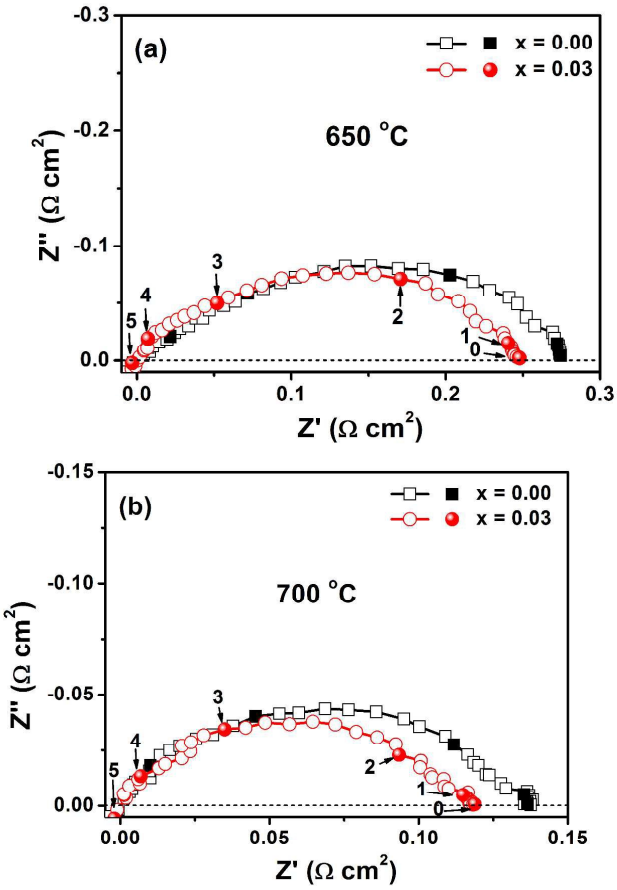

Figure 10 Impedance spectra of $PrBa_{1-x}Fe_2O_{5+\delta}$/GDC/$PrBa_{1-x}Fe_2O_{5+\delta}$ symmetrical cells measured at 650 °C (a) and 700 °C (b) in air. Numbers in these plots correspond to logarithm of frequency.

3.8 Single cell performance

Figure 11 presents the I-V and I-P curves of the $PrBa_{1-x}Fe_2O_{5+\delta}$ based anode support single cells with the configuration of Ni-YSZ/YSZ/GDC/$PrBa_{1-x}Fe_2O_{5+\delta}$. The single cells were fabricated and tested with the same procedure to ensure the comparability of the presently obtained electrochemical performance data. The $PrBa_{0.97}Fe_2O_{5+\delta}$ based single cell exhibits the

maximum power densities of 329, 256, 183 and 118 mW cm^{-2} at 800, 750, 700 and 650 ^{o}C, respectively. These values are much higher than that of $PrBaFe_2O_{5+\delta}$ based single cell which indicate that the introduction of proper amount of Ba deficient can efficiently enhance the electrochemical performance of the cobalt-free double perovskite $PrBa_{1-x}Fe_2O_{5+\delta}$. $PrBa_{0.97}Fe_2O_{5+\delta}$ is a potential cathode material for IT-SOFCs.

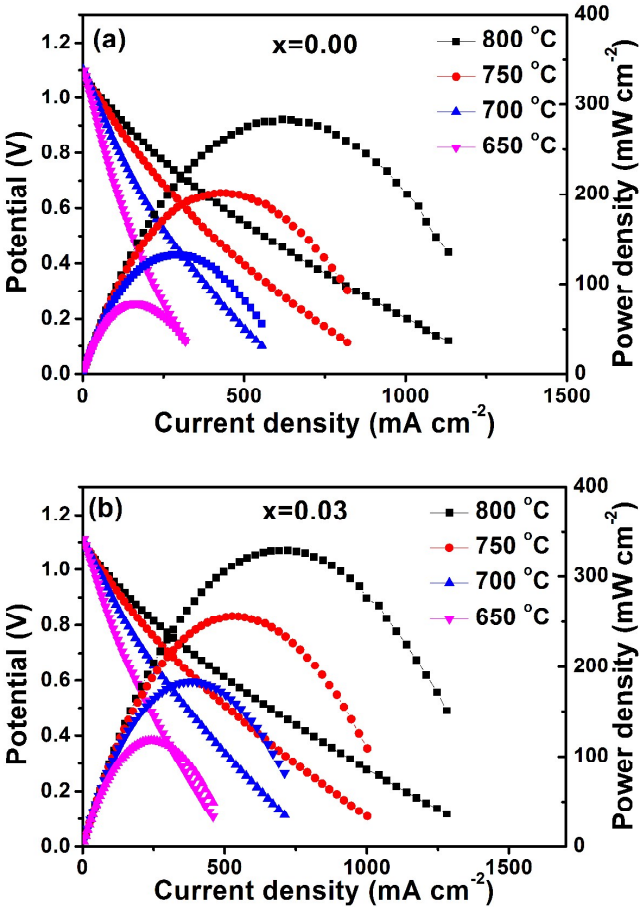

Figure 11 I-V and I-P curves of the (a) $PrBaFe_2O_{5+\delta}$ and (b) $PrBa_{0.97}Fe_2O_{5+\delta}$ based single cells.

4. Conclusions

Cobalt-free double perovskite $PrBa_{1-x}Fe_2O_{5+\delta}$ (x = 0.00–0.10) were synthesized and evaluated as a cathode material for IT-SOFCs with respect to the crystal structure, surface properties,

oxygen content, electrical conductivity, thermal expansion, chemical compatibility with GDC electrolyte, microstructure, and electrochemical performance. A layered structure with c approximately equal to 2a ≈ 2b and gradual shrinkage in the lattice with higher Ba deficiency (x) was observed for $PrBa_{1-x}Fe_2O_{5+\delta}$ oxides. Minor Pr_6O_{11} phase was detected for samples for which $x \geq 0.05$. Ba deficiency has little influence on the chemical state of O and Pr, but results in a slight reduction in transition metal (Fe) at surfaces of the sample. Iodometric titration and TGA results show that Ba-deficient $PrBa_{0.97}Fe_2O_{5+\delta}$ exhibits a lower oxygen content than the parent $PrBaFe_2O_{5+\delta}$ at given temperature. An obvious decrease in electrical conductivity was obtained with higher x from 300–800 °C, which indicates that the formation of additional oxygen vacancies was the main charge compensation mechanism for Ba deficiency in the cobalt-free double perovskite $PrBa_{1-x}Fe_2O_{5+\delta}$. A slight decrease in TEC results from a Ba deficiency from 30–900 °C. The catalytic activity for the ORR of the cobalt-free double perovskites can be enhanced by introducing the appropriate amount of Ba deficiency, and is characterized by a decreased ASR compared with the parent oxide. ASR values as low as 0.119 Ω cm^2 were obtained for $PrBa_{0.97}Fe_2O_{5+\delta}$ at 700 °C. The $PrBa_{0.97}Fe_2O_{5+\delta}$ based single cell exhibits the maximum power densities of 329 and 183 mW cm^{-2} at 800 and 700 ^oC, respectively. These results suggest $PrBa_{0.97}Fe_2O_{5+\delta}$ is a potential cathode material for IT-SOFCs.

Acknowledgement

This work was financially supported by the National Natural Science Foundation of China (51402127, 51474037, 51474113), the Natural Science Foundation of Jiangsu Province

(SBK201341159), the China Postdoctoral Science Foundation (2014M550269, 2015T80524) and the Senior Talent Foundation of Jiangsu University (13JDG009).

References

1 E. D. Wachsman, and K. T. Lee, *Science*, 2011, **334**, 935-939.

2 B. C. H. Steel, and A. Heinzel, *Nature*, 2001, **414**, 345-352.

3 A. A. Taskin, A. N. Lavrov, and Y. Ando, *Appl. Phys. Lett.*, 2005, **86**, 091910.

4 A. A. Taskin, A. N. Lavrov, and Y. Ando, *Appl. Phys. Lett.*, 2005, **86**, 134414.

5 A. Tarancon, M. Burriel, J. Santiso, S. J. Skinner, and J. A. Kilner, *J. Mater. Chem.*, 2010, **20**, 3799-3813.

6 J. -H. Kim, and A. Manthiram, *J. Electrochem. Soc.*, 2008, **155**, B385-B390.

7 E. Chavez, M. Mueller, L. Mogni, and A. Caneiro, *J. Physics: Conference Series*, 2009, **167**, 012043.

8 S. L. Pang, X. N. Jiang, X. N. Li, Q. Wang, and Z. X. Su, *J. Power Sources*, 2012, **204**, 53-59.

9 S. L. Pang, X. N. Jiang, X. N. Li, Z. X. Su, H. X. Xu, Q. L. Xu, et al., *Int. J. Hydrogen Energy*, 2012, **37**, 6836-6843.

10 K. Zhang, L. Ge, R. Ran, Z. P. Shao, and S. M. Liu, *Acta Mater.*, 2008, **56**, 4876-4889.

11 Y. J. Niu, W. Zhou, J. Sunarso, L. Ge, Z. H. Zhu, and Z. P. Shao, *J. Mater. Chem.*, 2010, **20**, 9619-9622.

12 Q. J. Zhou, T. Wei, S.Q. Guo, X. L. Qi, R. F. Ruan, Y. Li, et al., *Ceram. Int.,* 2012, **38**, 2899-2903.

13 L. Zhao, J. C. Shen, B. B. He, F. L. Chen, and C. R. Xia, *Int. J. Hydrogen Energy*, 2011, **36**, 3658-3665.

14 X. J. Xue, and H. P. Ding, *J. Power Sources*, 2010, **195**, 7038-7041.

15 D. J. Chen, F. C. Wang, H. G. Shi, R. Ran, and Z. P. Shao, *Electrochim. Acta*, 2012, **78**, 466-474.

16 J. Zou, J. Park, B. Kwak, H. Yoon, and J. Chung, *Solid State Ionics*, 2012, **206**, 112-119.

17 Y. N. Kim, J. -H. Kim, and A. Manthiram, *J. Power Sources*, 2010, **195**, 6411-619.

18 X. J. Xue, and H. P. Ding, *J. Power Sources*, 2010, **195**, 4718-4721.

19 X. J. Xue, and H. P. Ding, *J. Power Sources*, 2010, **195**, 4139-4142.

20 Z. Liu, L. Z. Cheng, and M. F. Han, *J. Power Sources*, 2011, **196**, 868-871.

21 Z. B. Yang, M. F. Han, P. Y. Zhu, F. Zhao, and F. L. Chen, *Int. J. Hydrogen Energy*, 2011, **36**, 9162-9168.

22 S. L. Pang, X. N. Jiang, X. N. Li, H. X. Xu, L. Jiang, Q. L. Xu, et al., *J. Power Sources*, 2013, **240**, 54-59.

23 S. L. Pang, X. N. Jiang, X. N. Li, Q. Wang, Z. X. Su, and Q. Y. Zhang, *Int. J. Hydrogen Energy*, 2012, **37**, 3998-4001.

24 F. F. Dong, M. Ni, Y. B. Chen, D. J. Chen, M. O. Tadé, and Z. P. Shao, *J. Mater. Chem. A*, 2014, **2**, 20520-20529.

25 J. P. Wang, F. C. Meng, T. Xia, Z. Shi, J. Lian, C. B. Xu, et al., *Int. J. Hydrogen Energy*, 2014, **39**,18392-18404.

26 W. Zhou, Z. P. Shao, W. Q. Jin, and N. P. Xu, *J. Power Sources*, 2008, **182**, 24-31.

27 E. -L. Rautama, P. Boullay, A. K. Kundu, V. Caignaert, V. Pralong, M. Karppinen, et al., *J.*

Mater. Chem., 2008, **20**, 2742-2750.

28 S. L. Pang, X. N. Jiang, X. N. Li, Q. Wang, and Q. Y. Zhang, *Mater. Chem. Phys.*, 2012, **131**, 642-646.

29 M. Ghaffari, M. Shannon, H. Hui, O. K. Tan, and A. Irannejad, *Surf. Sci.*, 2012, **606**, 670-677.

30 F. J. Jin, Y. Shen, R. Wang, and T. M. He, *J. Power Sources*, 2013, **234**, 244-251.

31 H. Falcón, J. A. Barbero, G. Araujo, M. T. Casais, M. J. Martínez-Lope, J. A. Alonso, et al., *Appl. Catal. B: Environ.*, 2004, **53**, 37-45.

32 L. L. Zhang, Q. J. Zhou, Q. He, and T. M. He, *J. Power Sources*, 2001, **195**, 6356-6366.

33 F. J. Jin, H. W. Xu, W. Long, Y. Shen, and T. M. He, *J. Power Sources*, 2013, **243**, 10-18.

34 S. B. Adler, *Chem. Rev.*, 2004, **104**, 4791-4843.

35 Z.P. Shao, and S. M. Haile, *Nature*, 2004, **431**, 170-173.

36 S. L. Pang, X. N. Jiang and X. N. Li, *Ferroelectrics*, 2015, **478**, 26-39.

37 L. Zhao, B. B. He, X. Z. Zhang, R. R. Peng, G. Y. Meng, and X. Q. Liu, *J. Power Sources*, 2010, **195**, 1859-1861.

38 Y. H. Ling, L. Zhao, B. Lin, Y. C. Dong, X. Z. Zhang, G. Y. Meng, et al., *Int. J. Hydrogen Energy*, 2010, **35**, 6905-6910.

39 K. K. Hansen, and K. V. Hansen, *Solid State Ionics*, 2007, **178**, 1379-1384.

40 G. Y. Zhu, X. H. Fang, C. R. Xia, and X. Q. Liu, *Ceram. Int.* 2005, **31**, 115-119.

41 B. Wei, Z. Lu, X. Q. Huang, M. L. Liu, N. Li, W. H. Su, *J. Power Sources*, 2008, **176**, 1-8.

42 F. J. Jin, Y. Shen, R. Wang, and T. M. He, *J. Power Sources*, 2013, **234**, 244-251.

43 S. H. Jo, P. Muralidharan, and D. K. Kim, *Electrochem. Commun.*, 2009, **11**, 2085-2088.

44 D. Parfitt, A. Chroneos, A. Tarancón, and J. A. Kilner, *J. Mater. Chem.*, 2011, **21**, 2183-2186.

45 M. Burriel, J. P. Martínez, R. J. Chater, S. Fearn, A. V. Berenov, S. J. Skinner, et al., *Chem. Mater.* 2012, **24**, 613-621.

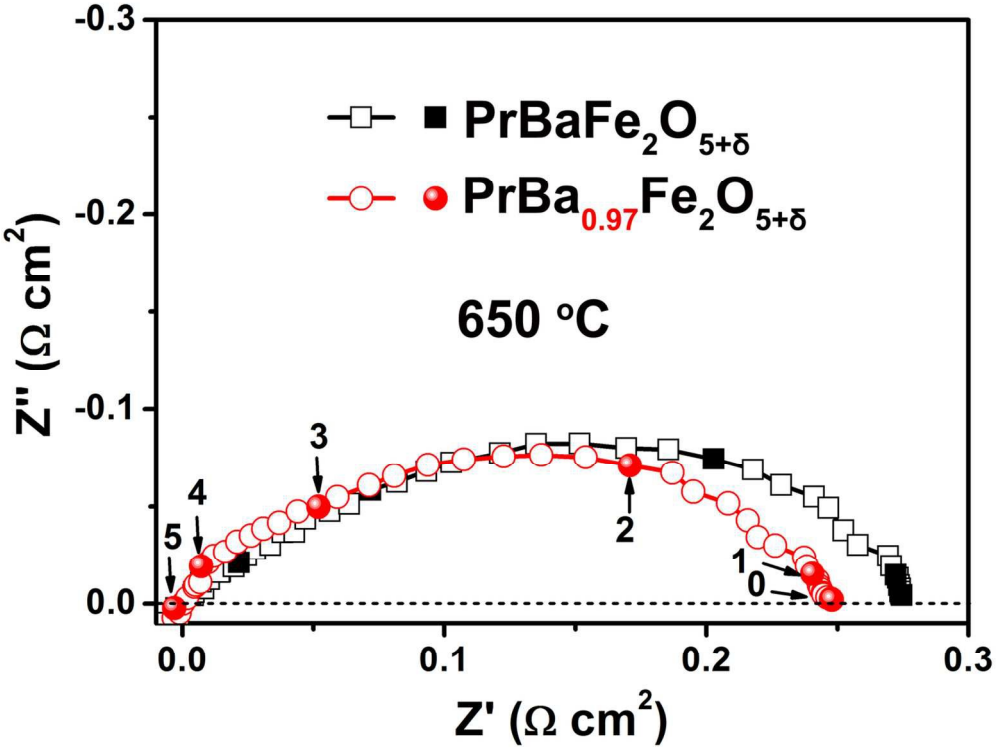

62x47mm (600 x 600 DPI)